



AIAA 2002-4511
Prediction of the Nonlinear
Aerodynamic Characteristics of
Tandem-control and Rolling-tail Missiles

D. Lesieutre, J. Love, and M. Dillenius
Nielsen Engineering & Research, Inc.
Mountain View, CA

AIAA Atmospheric Flight Mechanics
Conference
5-8 August 2002 / Monterey, CA

For permission to copy or republish, contact the copyright owner named on the first page.
For AIAA-held copyright, write to AIAA Permissions Department,
1801 Alexander Bell Drive, Suite 500, Reston, VA, 20191-4344.

PREDICTION OF THE NONLINEAR AERODYNAMIC CHARACTERISTICS OF TANDEM-CONTROL AND ROLLING-TAIL MISSILES

Daniel J. Lesieutre^{*}, John F. Love[†], Marnix F. E. Dillenius[‡]
Nielsen Engineering and Research, Inc.
Mountain View, CA 94043

ABSTRACT

Predicted nonlinear aerodynamic characteristics of several canard-body-tail missile models are presented and compared to wind tunnel data. Configurations with both fin sets deflectable (tandem-control) are analyzed to investigate the effectiveness of canard-only, tail-only, and combined tandem-control effectiveness for both vertical translation and pitch attitude changes. Configurations with canard control fins and free-rolling tail fin sections are investigated for their ability to minimize vortex-induced lateral forces and moments associated with canard control. Engineering- and intermediate-level aerodynamic prediction codes are used for the analysis. Results presented include high angle of attack aerodynamics, induced lateral forces, tandem-control fin deflections, estimates of free rotating fin section performance, and rotational damping estimates. Good agreement with experimental data is obtained for a variety of nonlinear and asymmetric flight conditions.

LIST OF SYMBOLS

| | |
|----------------|---|
| a | body radius at fin mid-rootchord |
| AR | aspect ratio (two fins joined at root) |
| C_{dc} | body crossflow drag coefficient |
| C_l | rolling moment/ $q_\infty S_R l_R$ |
| C_{lp} | roll-damping coefficient; $\partial C_l / \partial (p l_R / 2V_\infty)$ |
| C_m | pitching moment/ $q_\infty S_R l_R$; positive nose up |
| C_N | normal force/ $q_\infty S_R$ |
| C_{NF} | fin normal force/ $q_\infty S_R$ |
| $C_{N\alpha}$ | body $dC_N/d\alpha$ at $\alpha=0$ |
| D | body diameter, maximum |
| L | body length |
| l_R, l_{REF} | reference length |
| p, q, r | rotational rates, rads/sec |
| s | exposed fin span |
| s_m | fin semispan measured from body centerline |
| S_R | reference area |
| x_{CP} | center of pressure |
| x_{MC} | moment center |
| α_c | included angle of attack, deg |

| | |
|-------------|--|
| δ | fin deflection angle, deg |
| λ | fin taper ratio |
| ϕ | roll angle, deg |
| ϕ_{F2} | fin set roll angle with respect to body-fixed vertical axis, positive right wing down, deg |

INTRODUCTION

Recently, experimental data obtained by NASA personnel has become available for tandem-control missile configurations.^{1,2} These data exhibit many nonlinear characteristics associated with vortical interaction between fin sets. In addition, there are several sets of experimental data taken for canard-controlled missile models with fixed and free-rolling tail sections.^{3,4} These data also exhibit nonlinearities associated with strong canard-tail vortical interference including induced lateral forces and moments. An initial investigation of the ability of an engineering-level aerodynamic prediction code to predict the characteristics of these configurations has been presented.² This paper is aimed at investigating these configurations in more detail, using both engineering-level and intermediate-level aerodynamic prediction codes.

TECHNICAL APPROACH

This section summarizes the experimental data and the prediction methodology employed in this investigation. The estimation of rolling-tail section properties is also presented.

DESCRIPTION OF MISL3

The engineering-level missile aerodynamic prediction code *MISL3*² has been developed for aerodynamic performance prediction and for preliminary design of conventional missiles. The method uses the Triservice systematic fin-on-body force and moment data base^{4,5} The prediction methodology employed covers a Mach number range from 0.5 to 5.0, fin aspect ratios from 0.25 to 10.0, angles of attack to $\pm 90^\circ$, arbitrary roll angles, and deflection angles from -40° to 40° . The method uses the equivalent angle of attack concept

^{*} Senior Research Engineer, Senior Member AIAA

[†] Research Engineer

[‡] President, Associate Fellow AIAA

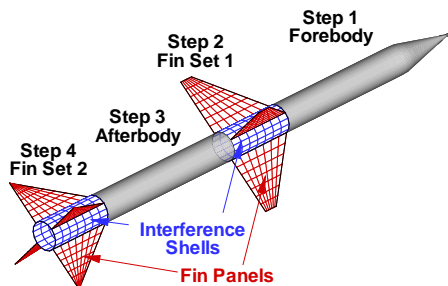
Copyright ©2002 by Nielsen Engineering & Research, Inc.

Published by the American Institute of Aeronautics and Astronautics, Inc. with permission.

which includes the effects of vorticity and geometric scaling. The current version of the *MISL3* program has been developed by extending the methodology to model conical changes in body diameter (flares, boattails) and to allow arbitrary interdigitation angles between fin sets. This, in combination with the roll rate capability of the code, allows estimation of the performance of configurations with rolling fin sets. Reference 2 provides more details regarding the methodology employed by *MISL3* and presents comparisons to experimental data for a wide variety of configurations.

DESCRIPTION OF MISDL

The intermediate-level aerodynamic prediction code *MISDL*^{6,7} is based on panel methods and other singularity methods enhanced with models for nonlinear vortical effects. The body of the missile is modeled by either subsonic or supersonic sources/sinks and doublets for volume and angle of attack effects, respectively. The fin sections are modeled by a horseshoe-vortex panel method for subsonic flow and by first-order constant pressure panels for supersonic flow. Up to three fin sections can be modeled and nonlinear fin and body vortices are modeled. The body vorticity is modeled using the VTXCHN vortex-cloud method described in Refs. 6-8. The overall calculation proceeds as follows: 1) the VTXCHN module is used to compute the forebody loads including vortex shedding and tracking, 2) loads within the fin set are calculated including the effects of forebody vorticity, 3) the vorticity shed from the forebody and the forward fin set is included as an initial condition in VTXCHN module which tracks and models additional vortices shed from the afterbody, and 4) if second or third fin sets are present, steps 2 and 3 are repeated. A schematic of the calculation procedure and paneling layouts is shown in the following sketch.



The range of parameters of the *MISDL* code include: Mach numbers from 0.0 to 3.0 with a modified shock-expansion capability to higher supersonic speeds, angles of attack up to 20 degrees, arbitrary roll angles, rotational rate effects, and nonuniform flow effects.

MISDL can model noncircular body configurations and configurations with unconventional fin shapes. A recent extension of the code enabled the modeling of the subsonic Penguin missile with canards on the nose and deployed and folded wings.⁶ A version of *MISDL* employing an optimizer was used to design unconventional fin planforms for several design objectives including minimization of fin hinge moments and maximization of normal force.⁹

ROLLING-TAIL CHARACTERISTICS

Estimation of the aerodynamic characteristics of the rolling tail section including tail section roll rate follows. The roll equation of motion for the tail section as a function of time t is:

$$T = T_{AF}(t) + T_{AD}(t) + T_{BF}(t) = I_X(dp/dt) \quad (1)$$

where T is torque and I_X is the moment of inertia in roll of the tail section. The subscript designations are:

- AF - aerodynamic forcing,
- AD - aerodynamic damping, and
- BF - bearing friction (or brake force).

The time-dependent aerodynamic forcing torque on the tail fins, $T_{AF}(t)$, is caused by the aerodynamic fin forces which are dependent on the angle of attack and the fin section roll angle, ϕ_{F2} . The aerodynamic damping torque, $T_{AD}(t)$, is dependent on the tail section roll rate and the angle of attack. The third torque, T_{BF} , can be used to model bearing friction and/or braking torque.

In this paper, the rolling tail characteristics are estimated based on static characteristics and calculated roll damping characteristics. The analysis of Falanga¹⁰ is followed. For steady-state conditions (constant roll rate, no variance with ϕ_{F2}), the sum of the moments must be zero.

$$\sum \text{moments} = M_{AF} + M_{AD} + M_{BF} = 0 \quad (2)$$

Substituting $M_{AF} = C_l q_\infty S_R l_R$ and $M_{AD} = C_{lp} (\rho l_R / 2 V_\infty) q_\infty S_R l_R$

into Eqn. (2) and solving for the roll rate p , yields:

$$\frac{p l_R}{2 V_\infty} = - \frac{C_l}{C_{lp}} \left(1 + \frac{M_{BF}}{M_{AF}} \right) \quad (3)$$

For cases where the bearing torque is much smaller than the aerodynamic torque, the roll rate can be estimated as follows:

$$\frac{p_R^l}{2V_\infty} = -\frac{C_l}{C_{lp}} \quad \text{for } M_{BF} < M_{AF} \quad (4)$$

For a high quality bearing, this assumption is valid. Eqn. (4) is used to estimate the tail fin roll rate with predictions of C_l and C_{lp} . Conversely, Eqn. (4) is used to estimate the experimental tail section roll damping, C_{lp} , from the measurements of C_l and p . Eqn. (3) can be used to compare to rolling tail results with a brake-force applied.

RESULTS

This section presents longitudinal and lateral-directional aerodynamic predictions for several tandem-control configurations, and for configurations with canard-controlled fixed and free-to-roll tail sections. Predicted results obtained with engineering- and intermediate-level prediction codes are shown. Nonlinear aerodynamic characteristics associated with high angle-of-attack and asymmetric flow conditions are illustrated. Comparisons of predictions to the Tandem-Control Model data base are presented. The effects of interdigitation between fin sets is analyzed along with the estimation of tail fin section roll rate for a canard-tail configuration with a free-rolling tail section.

TANDEM CONTROL

Tandem-Control Model Experiment. Tandem-Control data presented in this section were obtained from tests conducted in the NASA/LaRC Unitary Plan Wind Tunnel at free-stream Mach numbers from 1.75 to 2.86.^{1,2} The test objective was to provide an aerodynamic database to study and evaluate tandem control effectiveness. The model consists of a 3-caliber ogive nose followed by a 12-caliber cylinder with cruciform inline canards and aft tail fins. Tests were performed on two models. Both models had the same canard fins, $AR = 1.6$ and $\lambda = 0.625$. The first model shown in Figure 1 had larger span tail fins, $AR = 2.33$ and $\lambda = 0.625$, and the second model tail fins identical to the canard fins, Figure 3. Model aerodynamic forces and moments were measured with an internally mounted six-component strain-gage balance. To assure turbulent flow over the model all tests were performed with boundary-layer transition strips located on the model nose and near the leading edges of the canard and tail fins. The test Reynolds number based on body diameter was 4.33×10^5 .

Tandem-Control Model Predictions. Figures 1 and 2 show measured and predicted¹ results for the Tandem-Control Model with larger span tail fins described

above. For $M_\infty = 1.75$ and $\phi = 0^\circ$, *MISL3* predictions are shown in Figure 1, and *MISDL* predictions are in Figure 2. Results are shown for four sets of horizontal fin deflections:

- 1) $\delta_{CANARD} = 0^\circ, \delta_{TAIL} = 0^\circ$
- 2) $\delta_{CANARD} = 10^\circ, \delta_{TAIL} = 5^\circ$
- 3) $\delta_{CANARD} = 10^\circ, \delta_{TAIL} = 10^\circ$
- 4) $\delta_{CANARD} = 5^\circ, \delta_{TAIL} = -5^\circ$

The zero deflection case is the reference. Cases 2) and 3) are deflections for vertical translation, and Case 4) is deflection for rotation in pitch. The normal force, pitching moment, center of pressure, and axial force as a function of α_c are all predicted very well by *MISL3*, Figure 1. The nonlinear characteristics of the pitching moment are predicted especially well by *MISL3*, and the center of pressure predicted is within a body radius of the measured values. The axial force characteristics are also predicted well. The *MISDL* predictions, Figure 2, are also predicted well with the largest errors occurring above 20° angles of attack.

The results in Figure 3 are for the Tandem-Control configuration with identical canard and tail fins described above. Figure 3 depicts the configuration and presents *MISL3* results for canard pitch control for $M_\infty = 1.75$ and $\phi = 45^\circ$. This case is shown because of the nonlinearities in the pitching moment which arise in the “X” orientation from canard vortices affecting the tail fins. *MISL3* predicts the nonlinear pitching moment characteristics well, and predicts the overall center of pressure to within a body radius for this configuration.

TWO-FIN SET CONFIGURATION WITH FREE-ROLLING TAIL SECTION

Figures 4 through 10 present results for a similar canard-tail missile model.³ The model has a 3-caliber tangent-ogive nose and an overall body length of 15 diameters. The test Reynolds number based on body diameter was 4.17×10^5 . Results for three test configurations are presented. For all configurations, the canards are in the $\phi_{F1} = 0^\circ$ orientation (“+” orientation, designated C+). Three tail section orientations were tested:

- 1) $\phi_{F2} = 0^\circ$ (“+” orientation, designated T+),
- 2) $\phi_{F2} = 45^\circ$ (“X” orientation, designated Tx), and
- 3) tail section free to rotate (designated T-free).

The C+Tx and C+T+ configurations are depicted in Figures 4 and 8, respectively. Results are presented for canard roll control and canard yaw control deflections.

The purpose of comparing to this experimental data was to investigate the predictive capabilities of the *MISL3* and *MISDL* codes and to gain insight into the aerodynamic characteristics of configurations with rolling tail sections. In this investigation, the codes were used to 1) estimate the static roll characteristics of the tail section under the influence of asymmetric canard vortices arising from roll and yaw control deflections, 2) estimate the roll damping characteristics of the tail section as a function of angle of attack, and 3) estimate the roll rate of the free-to-rotate tail section as a function of angle of attack.

Canard Roll Control. Figure 4 compares measured³ and predicted pitch plane aerodynamic characteristics for a Mach number of 1.7 with the horizontal canards deflected for roll control, $\delta_{\text{ROLL}} = -5^\circ$ ($\delta_{\text{ROLL}} = (\delta_{C_2} - \delta_{C_4})/2$). Measured and predicted results are shown for the C+T+ and C+Tx configurations. In addition, the measured data for the C+T-free configuration are also shown. The normal-force coefficient is predicted well for the C+T+ configuration. *MISL3* and *MISDL* somewhat underpredict the characteristics of the C+Tx configuration. The C+T+ pitching moment is in good agreement. The C+Tx pitching moment is overpredicted. For *MISL3*, the center of pressure is predicted within one body radius for both configurations except for small load conditions near $\alpha_c = 0^\circ$. *MISDL* predicts the center of pressure to within one body radius for C+Tx and within eight-tenths of a diameter for C+T+. The axial force is predicted well. The measured characteristics of the C+T-free configuration fall between the C+T+ and C+Tx characteristics.

Figure 5 compares measured and predicted rolling moment characteristics for the C+T+ and C+Tx configurations with canard roll control, $\delta_{\text{ROLL}} = -5^\circ$. In addition, the direct canard rolling moments predicted by *MISL3* and *MISDL* are compared to the C+T-free measured results. The free-to-rotate tails do not pass a rolling moment to the main balance, except through bearing friction forces which are very small. It is seen in Figure 5 that the predicted direct roll control is in very good agreement with the measured C+T-free rolling moment. *MISDL* slightly overpredicts the canard rolling moment. The *MISL3* predicted rolling moments for the C+T+ and C+Tx configurations agree well with data up to 4° angle of attack and have the correct trends above 4° . *MISDL* predicts the rolling moments for the C+T+ and C+Tx configurations very well in magnitude and trend.

This rolling moment is difficult to predict because it is dominated by the canard and body shed vortices influencing the tail fins. This is the classical induced

roll effect seen on canard-controlled missiles. For these configurations, the induced tail fin rolling moment opposes the direct canards control and actually causes the overall rolling moment to oppose the intent of the canard deflection.

Figure 6 shows the *MISL3* predicted crossflow velocity fields at the leading edge of the tail fin section for angles of attack of 0, 4, 8, and 12° . For $\alpha_c = 0^\circ$, Figure 6(a), it is seen that the canard vortices produce a counterclockwise swirling flow (looking forward) which produces the negative induced rolling moment on the tail fin section as seen in Figure 5. For $\alpha_c = 4^\circ$, Figure 6(b), the effects of the vortex shed from the right canard vortex is not apparent because it is lightly loaded ($\alpha_c + \delta_{C_2} = -1^\circ$). There is a stronger vortex on the left side corresponding to $\alpha_c + \delta_{C_4} = +9^\circ$. The flow field is asymmetric and results in a negative induced tail fin section rolling moment. The results for $\alpha_c = 8^\circ$, Figure 6(c), show a large vortex from the left canard and a weaker one from the right canard. The higher angle of attack results in the vortices tracking further above the body. There is still an asymmetric flow field which produces a negative tail section rolling moment for both the C+T+ and C+Tx configurations. Figure 6(c) also indicates the beginning of the body shed vorticity modeled by *MISL3*.

When $\alpha_c = 12^\circ$, Figure 6(d), the canard vortices have tracked to positions above the tail fin region, and significant body shed vorticity is present. The induced rolling moment on the tail fin section is small for this angle of attack for both the C+T+ and C+Tx configurations, but it has a positive slope as seen in Figure 5. Above 12° angle of attack, the predicted induced rolling moment from the tail fins is positive. The experimental data show this behavior to a lesser extent. In the prediction, this arises from the asymmetric body vorticity (produced due to asymmetric canard vorticity). The left-side body vorticity is weaker than the right-side; the result is an induced positive roll on the tail fins for both the C+T+ and C+Tx configurations. This is similar, but opposite, to the results at lower angles of attack with asymmetric canard vortices. Further insight is gained from these crossflow velocity predictions when the variation of tail section rolling moment as a function of interdigitation angle is discussed next in connection with Figure 7(a).

For the canards deflected $\pm 5^\circ$ for right-wing-down roll control (δ_{ROLL}), Figure 7(a) shows the predicted static rolling-moment coefficient of the tail fin section as a function of tail fin set roll angle ϕ_{F_2} . Results are shown for angles of attack of 0, 4, 8, and 12° . The tail fin rolling moment is negative (right fin up) for angles of

attack below 8° . This is apparent in the flow field predictions shown in Figures 6(a)-6(c) which show partially counterclockwise flow fields for $\alpha_c = 0$ and 4° . Above 4° angle of attack, a significant cyclic variation in C_l develops, Figure 7(a). For 12° , the rolling moment variation is cyclical and changes sign. The slope of C_l with respect to ϕ_{F2} (positive clockwise) at the zero crossings is such that the tail section “locks-in” to a zero roll rate when it is near the “X” orientation, $\phi_{F2} = 45, 135^\circ$.

To estimate the tail fin roll rate using Eqn. (4), C_l and C_{lp} must be estimated. C_l is estimated as the *mean* C_l with respect to ϕ_{F2} (see Figure 7(a)). The roll damping coefficient, C_{lp} , is estimated by running *MISL3* and *MISDL* with a nonzero roll rate (tail fins only) and computing C_{lp} . It was found that C_{lp} is constant for the range of roll rates under investigation (that is, C_l is linear with respect to p). However, there is a dependence on angle of attack as shown in Figure 7(b). The experiment did not measure the roll damping, but it was estimated using Eqn. (4) as follows:

$$C_{lp} = -\frac{\frac{1}{2}[C_l(C+T+)+C_l(C+Tx)]-C_l(C+T-free)}{\frac{p^l_r}{2V_\infty}} \quad (5)$$

where the rolling moment coefficients are given by the experimental values and the roll rate is the experimental value in radians per second.

For the predictions, tail fin roll rate is estimated as $-C_l/C_{lp}$ (Eqn. (4), and converted to rpm) and is shown in Figure 7(c). The magnitude of the roll rate is underpredicted by *MISL3* and overpredicted by *MISDL*. For both codes, the trends are predicted well. The characteristics of the rolling moment predicted with respect to ϕ_{F2} are such that the tail fins “lock-in” to a zero roll rate around 12° . The experimental results indicate that this happens at 14° as does *MISDL*. The predicted results are dependent on the prediction of C_l and C_{lp} for the tail section. These quantities are difficult to predict accurately, especially when they are influenced by upstream asymmetric vorticity.

Both *MISL3* and *MISDL* provide reasonable estimates of the roll rate characteristics of a free-to-roll tail section under the influence of the asymmetric flow field associated with canard roll control as a function of angle of attack.

Canard Yaw Control. Figure 8, 9, and 10 compare measured³ and predicted rolling moment aerodynamic characteristics for canards deflected for yaw control,

$\delta_{YAW} = -5^\circ$ ($\delta_{YAW} = (\delta_{C1} + \delta_{C3})/2$). Figures 8 and 9 compare measured and predicted rolling moment characteristics for the **C+T+** and **C+Tx** configurations, respectively. In addition, the canard-only rolling moments predicted by *MISL3* and *MISDL* are compared to the **C+T-free** measured results. Figure 10 compares predicted and measured tail section roll rate and estimated tail section roll damping.

The **C+T-free** results shown in Figure 8 or 9 show the rolling moment associated with the canards deflected for yaw. Near zero angle of attack, the rolling moment is zero. As the angle of attack is increased, a rolling moment develops due to top to bottom asymmetries in the nose flow field due to the presence of the body bow shock and to the flow expansion over the upper surface of the nose. The expansion over the upper surface of the nose results in a reduction in dynamic pressure in the region of the upper canard fin. This “shading” of the upper fin results in a net positive rolling moment for the canards alone. This effect is not predicted adequately by engineering-level and intermediate-level aerodynamic predictions code.

For the **C+T+** and **C+Tx** configurations *MISL3* and *MISDL* predict the rolling moment behavior well as seen in Figures 8 and 9. It is difficult to predict the nonlinear rolling moment because it is due to induced vortical interference of the canard vortices on the tail fins. For yaw control, the results are dependent on the path of the lower canard vortex past the tail fins. *MISL3* predicts the correct trend but underestimates the peak magnitude. *MISDL* predicts the low angle of attack characteristics well and tends to overestimate the rolling moment at higher angles. Overall, both *MISL3* and *MISDL* estimate rolling characteristics good enough for preliminary design estimates.

For the canards deflected -5° for nose-to-left yaw control (δ_{YAW}), Figure 10(a) shows the predicted static rolling-moment coefficient of the tail fin section as a function of tail fin set roll angle ϕ_{F2} . Results are shown for angles of attack of 0, 4, 8, and 12° . It is seen that the tail fin rolling moment has no zero crossings for angles of attack below 8° . Like the roll control results in Figure 7(a), above 4° angle of attack, a significant cyclic variation in C_l develops. For 12° , the rolling moment variation is cyclical and changes sign. The slope of C_l with respect to ϕ_{F2} (positive clockwise) at the zero crossings is such that the tail section “locks-in” to a zero roll rate when it is near the “X” orientation, $\phi_{F2} = 45, 135^\circ$.

To estimate the tail fin roll rate using Eqn. (4), C_l and C_{lp} must be estimated. C_l is estimated as the *mean* C_l

with respect to ϕ_{F2} (see Figure 10(a)). The roll damping coefficient, C_{lp} , shown in Figure 10(b) is estimated by running *MISL3* and *MISDL* with a nonzero roll rate (tail fins only) and by using Eqn. (5) to estimate the experimental value. The Mach number variation of the roll damping coefficient, C_{lp} , is predicted well by *MISL3*. *MISDL* underestimates C_{lp} for $M_\infty = 2.16$ and 2.86.

The tail fin roll rate is estimated as $-C_l/C_{lp}$ (Eqn. (4), and converted to rpm) and is shown in Figure 10(c). The roll rate p is inversely proportional to C_{lp} and is very sensitive to its estimation. For *MISDL*, the underestimation of C_{lp} for $M_\infty = 2.16$ and 2.86 results in an overprediction of roll rate. Neither *MISL3* nor *MISDL* predict the correct roll rate trend as a function of Mach number. The experiment indicates that the roll rate decreases with increasing Mach number which implies that C_l decreases faster than C_{lp} with increasing Mach number. A detailed study is required to further assess these effects. The predicted results are dependent on the prediction of *mean* C_l and C_{lp} for the tail section. These quantities are difficult to predict accurately, especially when they are influenced by upstream asymmetric vorticity.

Note that the characteristics of the rolling moment predicted with respect to ϕ_{F2} , Figure 10(a), are such that the tail fins “lock-in” to a zero roll rate around or above 12°. The experimental results indicate that this happens at 14°. The roll equation of motion given by Eqn. (1) would need to be integrated within *MISL3* and *MISDL* to determine when “lock-in” actually is predicted.

CONCLUSIONS

This paper describes the prediction of the nonlinear aerodynamic characteristics of missile configurations with tandem-controls and free-rolling tail sections. The extensive comparisons to experimental aerodynamic data include longitudinal and lateral aerodynamic characteristics including nonlinear vortex-induced effects. In general, the predicted aerodynamic characteristics are in good to excellent agreement with the experimental data and provide insight into understanding the nonlinear characteristics of missiles with free-to-rotate tail sections.

ACKNOWLEDGMENTS

NEAR would like to thank Mr. A. B. Blair, Jr., (retired) and Mr. Jerry M. Allen of NASA/LaRC for their assistance in obtaining the Tandem-Control wind tunnel data.

REFERENCES

1. The Tandem-Control Data taken by A. B. Blair, Jr., NASA Langley Research Center.
2. Lesieutre, D. J., Love, J. F., Dillenius, M. F. E., and Blair, A. B., Jr., “Recent Applications and Improvements to the Engineering-Level Aerodynamic Prediction Software *MISL3*,” AIAA 2002-0275, Jan. 2002.
3. Blair, A. B., Jr., “Wind-Tunnel Investigation at Supersonic Speeds of a Remote-Controlled Canard Missile With a Free-Rolling-Tail Brake Torque System,” NASA TP 2401, Mar. 1985.
4. Blair, A. B., Jr., “Supersonic Aerodynamic Characteristics of a Maneuvering Canard-Controlled Missile with Fixed and Free-Rolling Tail Fins,” SAE Paper 901993, Oct. 1990.
5. Allen, J. M., Shaw, D. S., and Sawyer, W. C., “Analysis of Selected Data From The Triservice Missile Data Base,” AIAA 89-0478, Jan. 1989.
6. Lesieutre, D. J., Dillenius, M. F. E., and Gjestvang, J., “Application of *MISDL/KDA* Aerodynamics Prediction Method to Penguin Missile,” AIAA 2002-0277, Jan. 2002.
7. Dillenius, M. F. E., Lesieutre, D. J., Hegedus, M. C., Perkins, S. C., Jr., Love, J. F., and Lesieutre, T. O., “Engineering-, Intermediate- and High-Level Aerodynamic Prediction Methods and Applications,” *Journal of Spacecraft and Rockets*, Vol. 36, No. 5, Sep.-Oct. 1999, pp. 609-620.
8. Hegedus, M. C., Dillenius, M. F. E., Perkins, S. C., Jr., and Mendenhall, M. R., “Improved Version of the VTXCHN Code,” NEAR TR 498, Aug. 1995.
9. Lesieutre, D. J., Dillenius, M. F. E., and Lesieutre, T. O., “Multidisciplinary Design Optimization of Missile Configurations and Fin Planforms for Improved Performance,” AIAA 98-4890, Sep. 1998.
10. Falanga, R. A., “Supersonic Investigation of a Spinning and Nonspinning Model of a Cajun (or Apache) Rocket Vehicle With Roll-Control Tabs,” NASA TN D-2576, Jan. 1965.

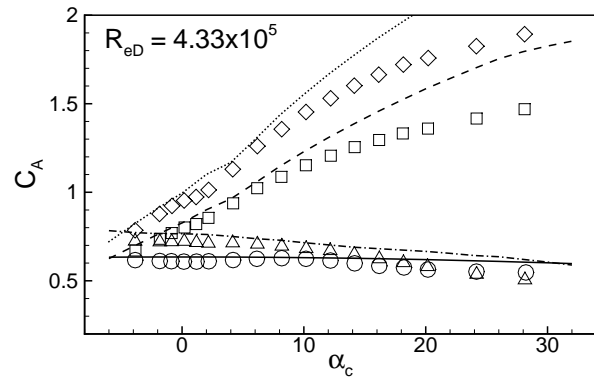
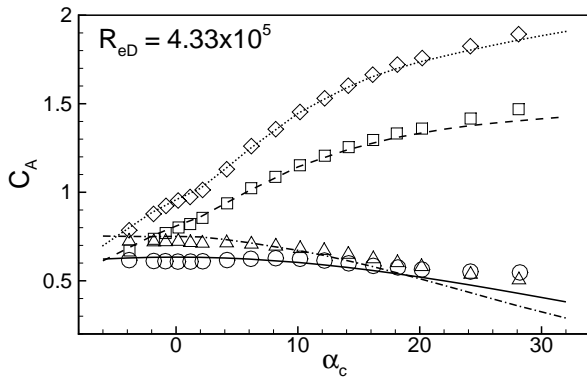
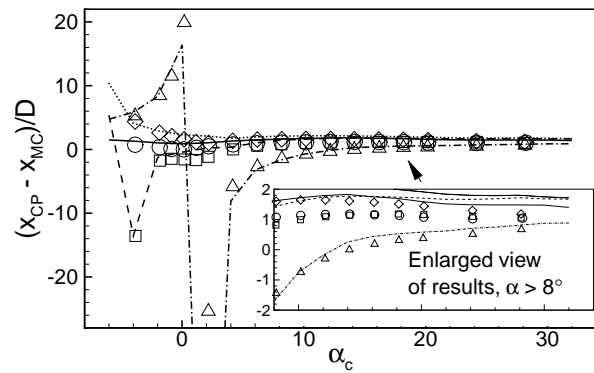
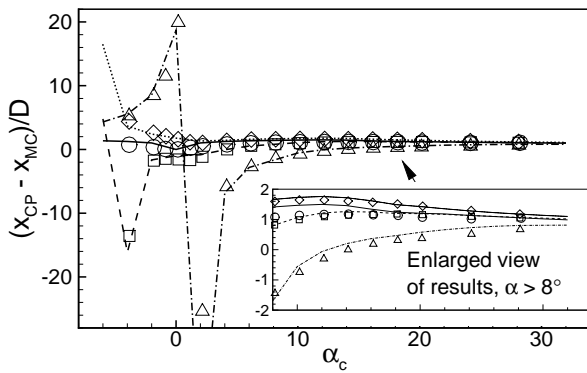
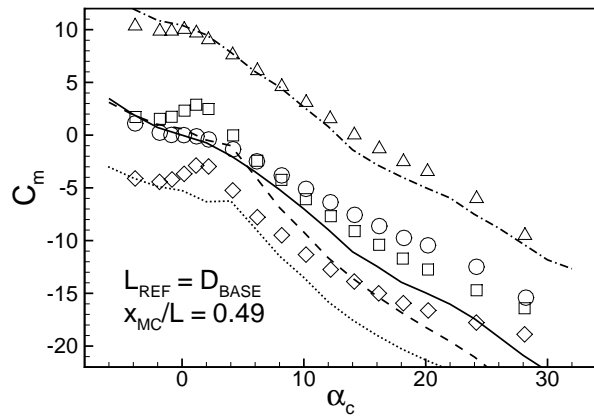
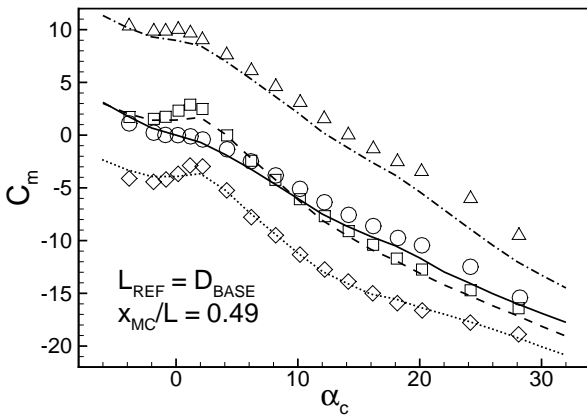
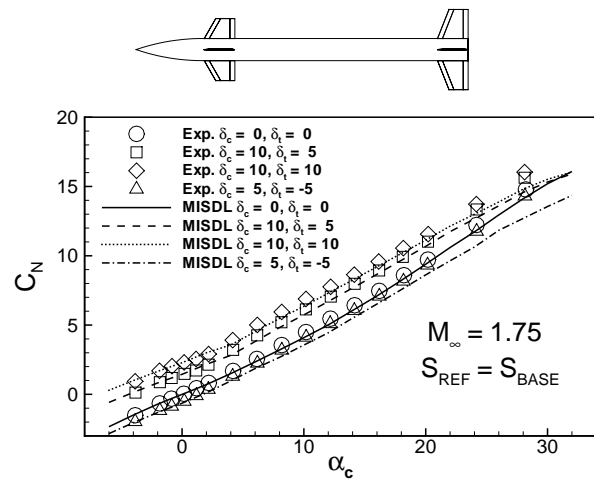
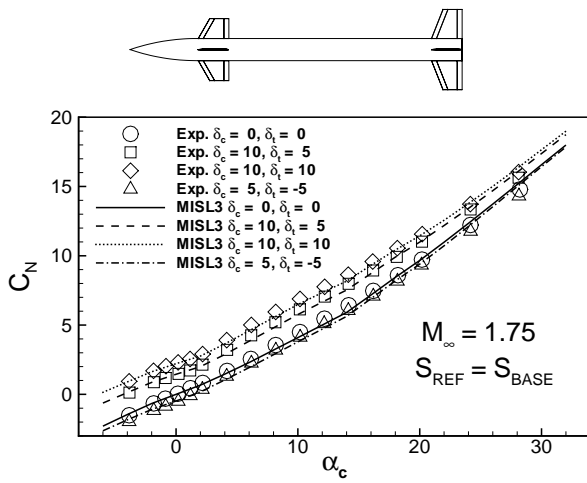


Figure 1.- Comparison of measured and MISL3 predicted aerodynamic characteristics for a tandem-control missile; $M_\infty = 1.75$, $\phi = 0^\circ$, Ref. 1.

Figure 2.- Comparison of measured and MISDL predicted aerodynamic characteristics for a tandem-control missile; $M_\infty = 1.75$, $\phi = 0^\circ$, Ref. 1.

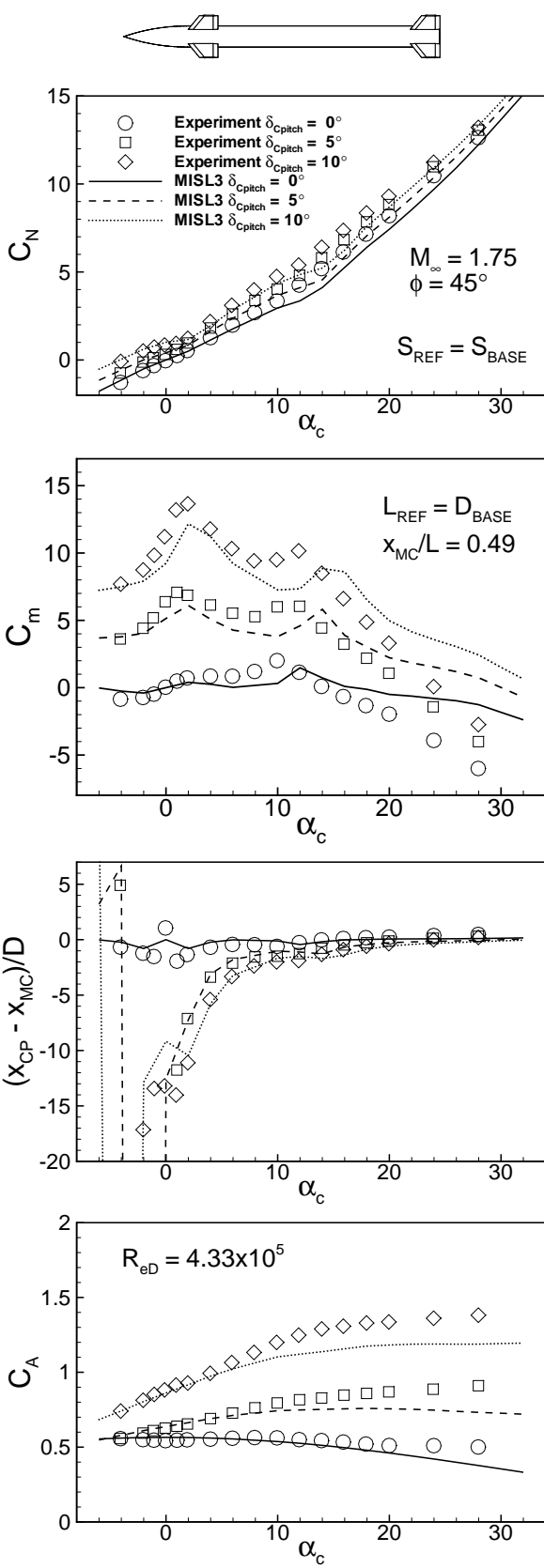


Figure 3.- Comparison of measured and MSL3 predicted aerodynamic characteristics, canard pitch control for $\phi = 45^\circ$, $M_\infty = 1.75$, Ref. 1.

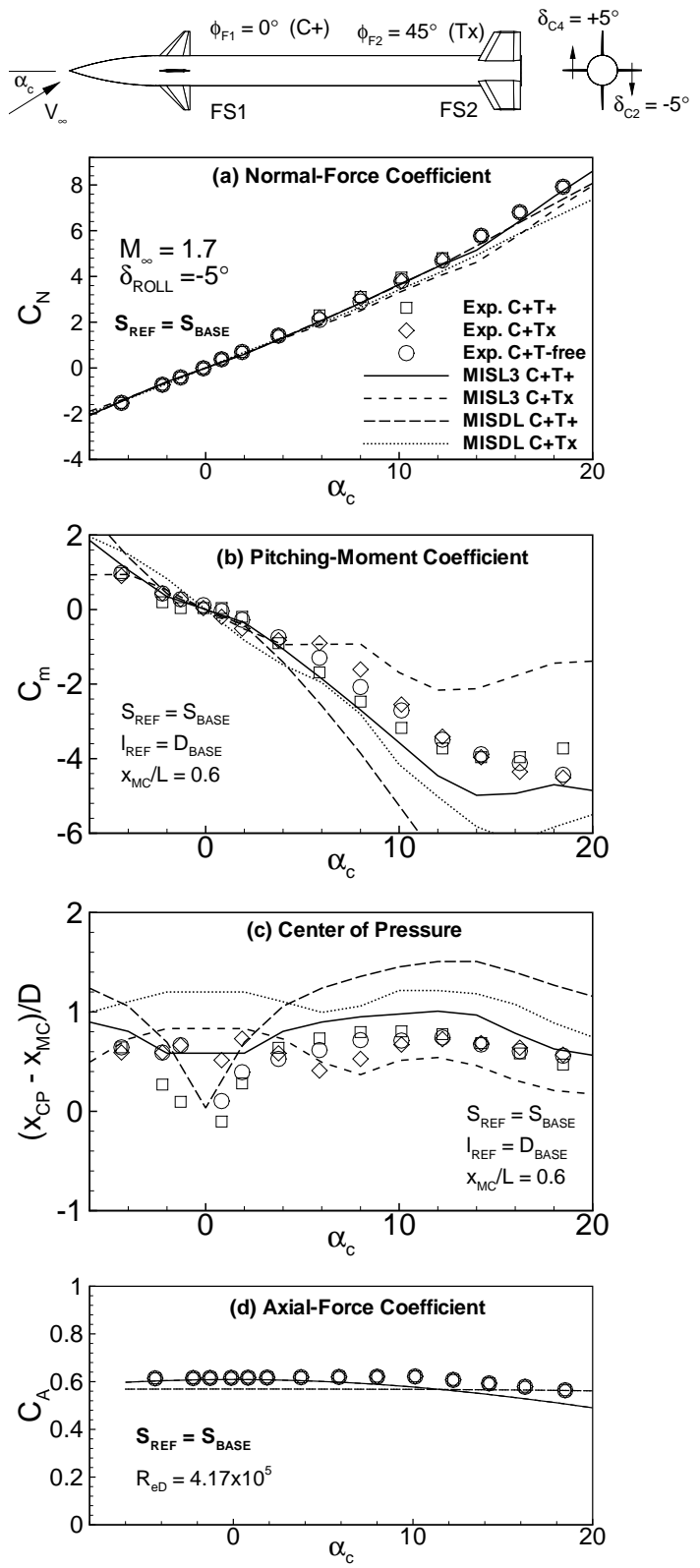


Figure 4.- Comparison of predicted and measured pitch-plane aerodynamic characteristics of a canard-tail configuration (Ref. 3) with: 1) tails in line with canards (C+T+), 2) tails interdigitated 45° (C+Tx), and 3) tails free to rotate (C+T-free).

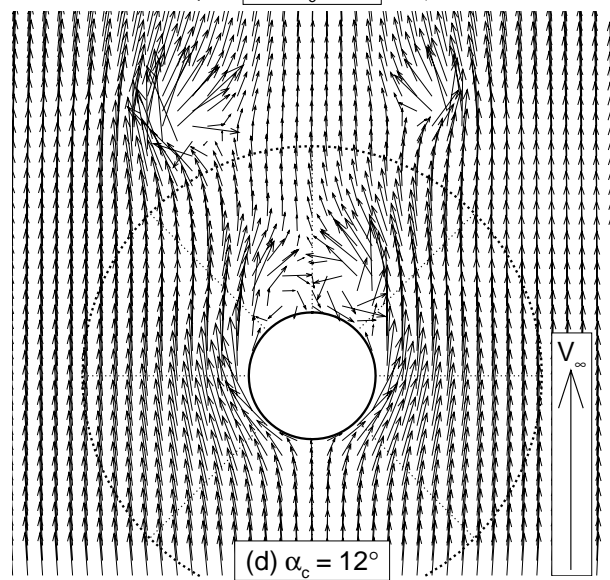
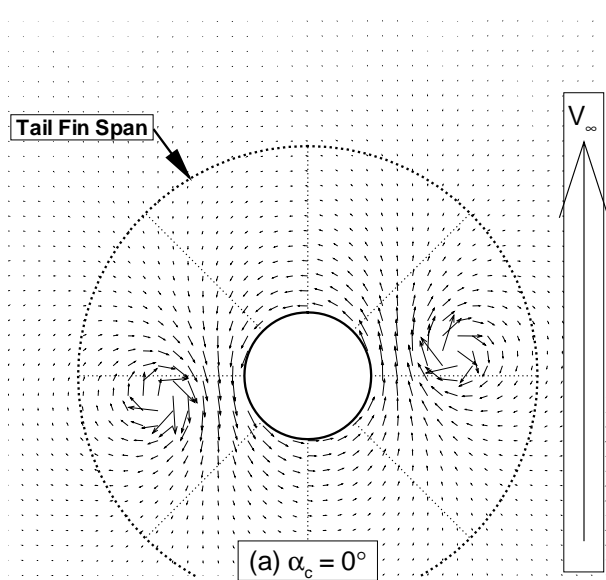
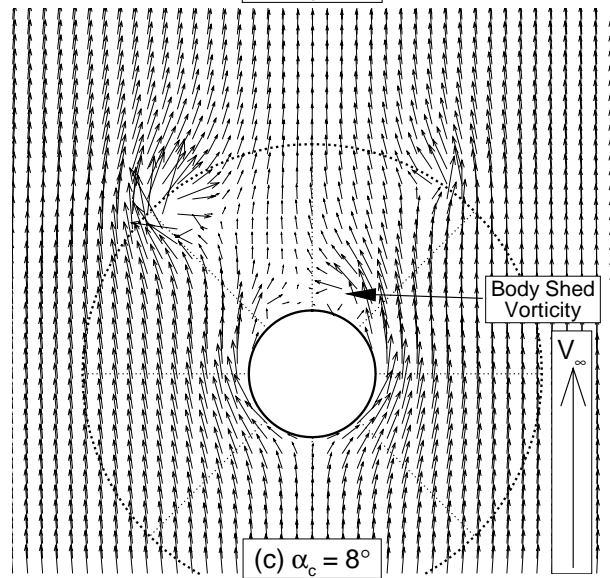
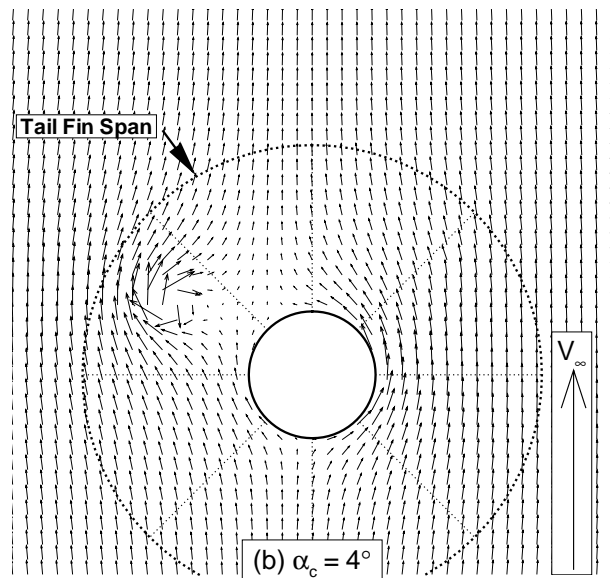
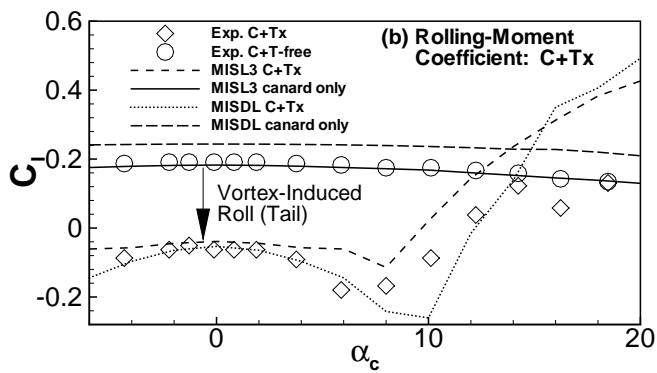
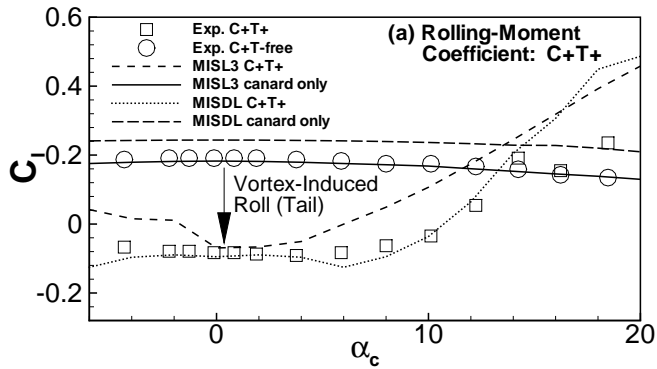
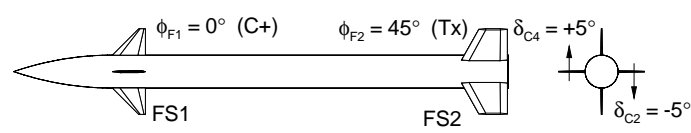


Figure 5.- Comparison of predicted and measured rolling-moment aerodynamic characteristics of a canard-tail configuration (Ref. 3) with:
 1) tails in line with canards (C+T+),
 2) tails interdigitated 45° (C+Tx), and
 3) tails free to rotate (C+T-free).

Figure 6.- Predicted crossflow velocity fields at the leading edge of the tail fin section,
 $M_\infty = 1.7$, $\delta_{C2} = -5^\circ$, $\delta_{C4} = +5^\circ$.

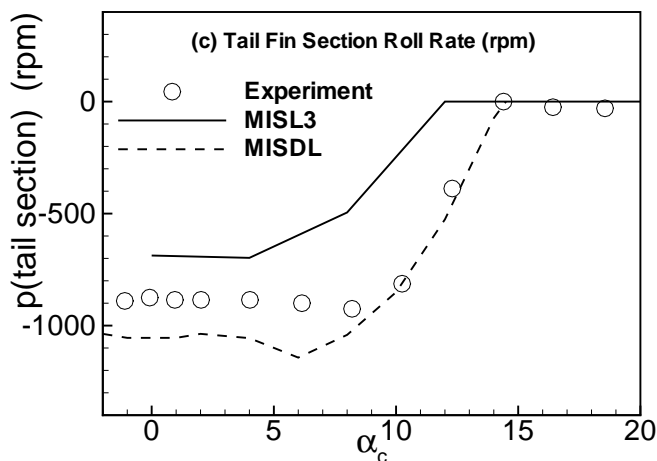
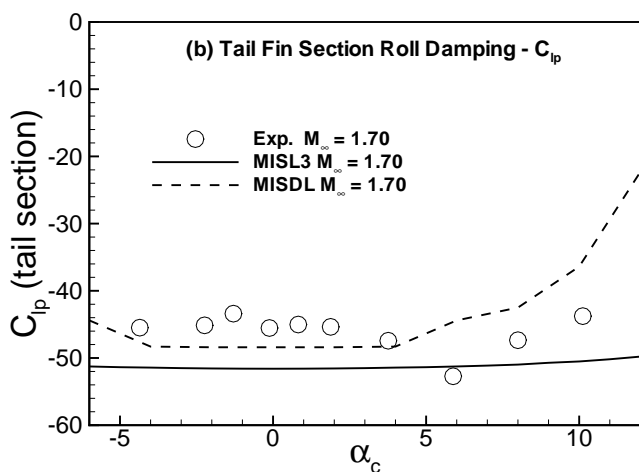
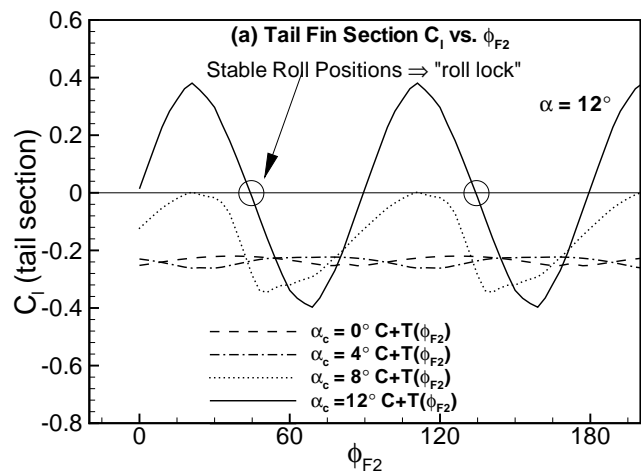
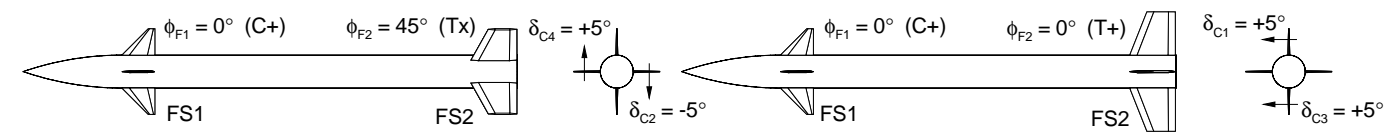


Figure 7.- Comparison of predicted and measured tail section aerodynamic characteristics, $M_\infty = 1.7$, $\phi = 0^\circ$, $\delta_{C2} = -5^\circ$, $\delta_{C4} = +5^\circ$, tail free to rotate, Ref. 3.

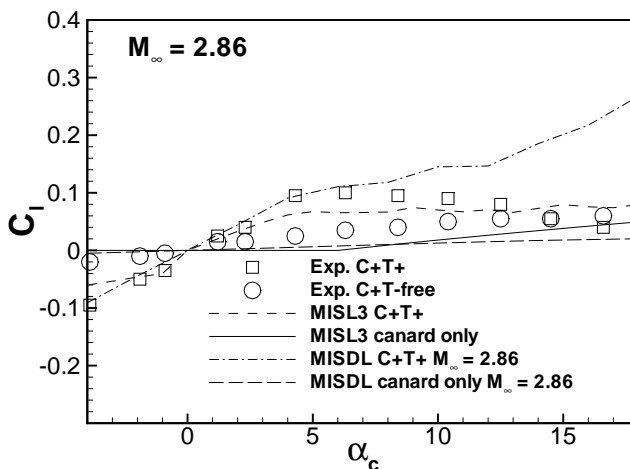
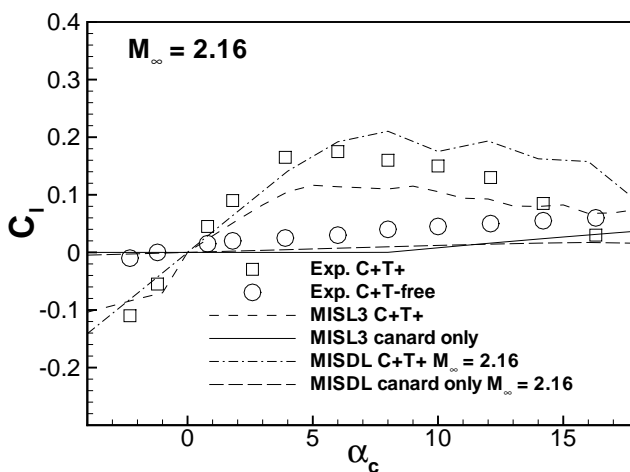
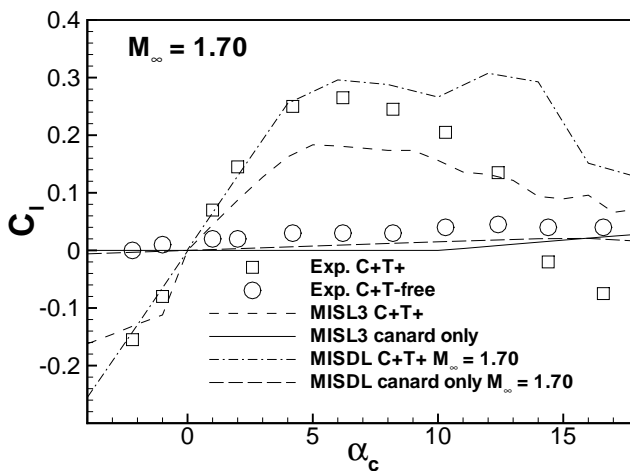


Figure 8.- Comparison of predicted and measured rolling-moment aerodynamic characteristics of a canard-tail configuration (Ref. 3) with canard yaw control: C+T+ and C+T-free. $\delta_{YAW} = -5^\circ$, $M_\infty = 1.70, 2.16, 2.86$.

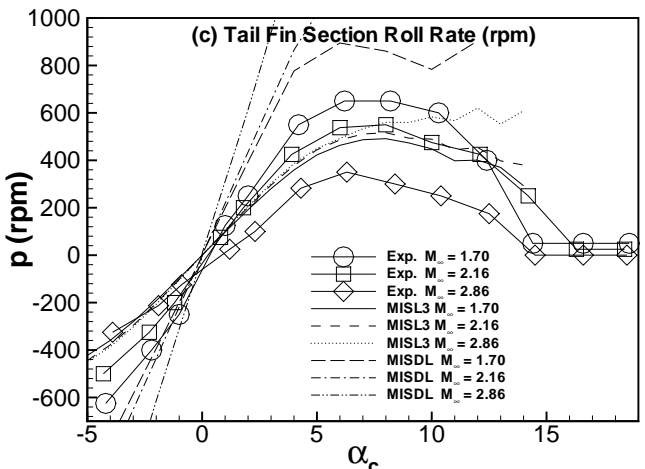
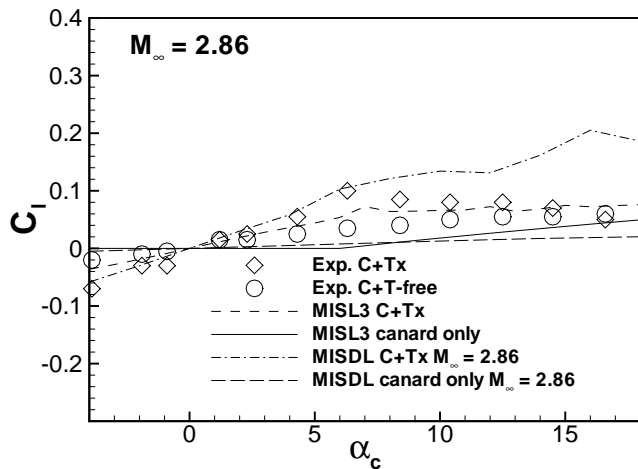
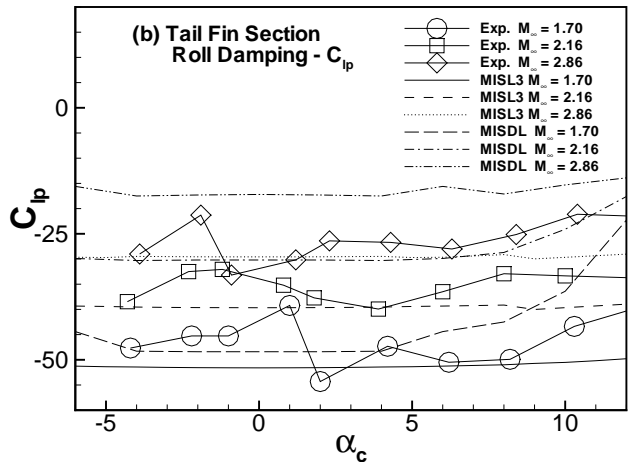
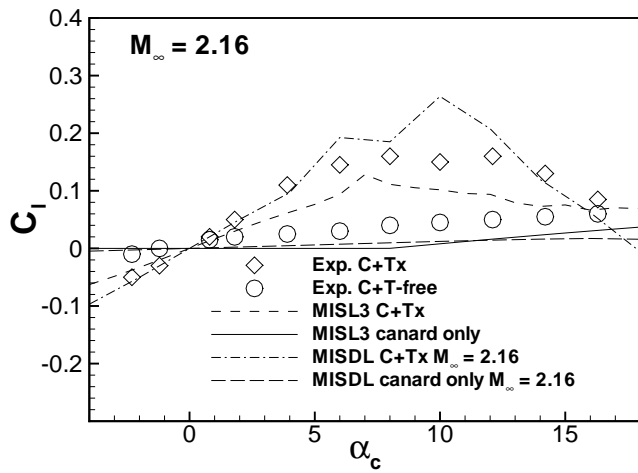
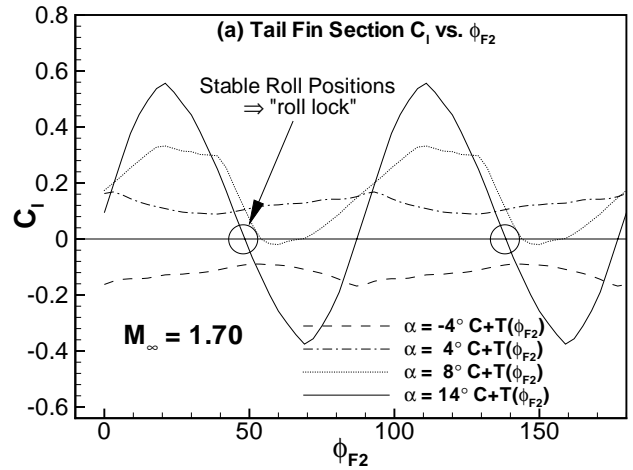
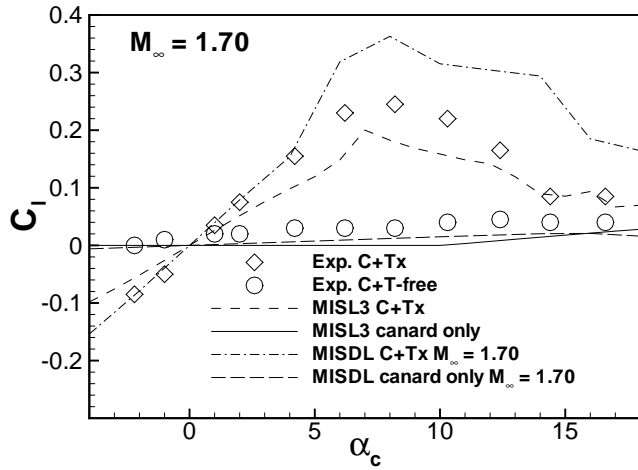
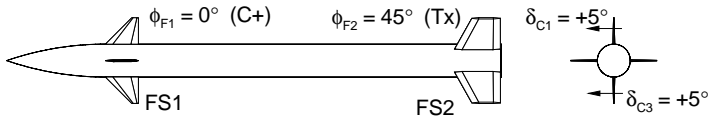


Figure 9.- Comparison of predicted and measured rolling-moment aerodynamic characteristics of a canard-tail configuration (Ref. 3) with canard yaw control: C+Tx and C+T-free. $\delta_{YAW} = -5^\circ$, $M_\infty = 1.70, 2.16, 2.86$.

Figure 10.- Comparison of predicted and measured tail section aerodynamic characteristics, $M_\infty = 1.70, 2.16, 2.86$, $\phi = 0^\circ$, $\delta_{YAW} = -5^\circ$, tail free to rotate, Ref. 3.